https://doi.org/10.2352/ISSN.2169-4451.2019.35.94

Design and Digital Fabrication of Magneto-dielectric Composites for Additive Manufacturing of Gradient Index RF Lenses

Khalid Masood[1], Tatiana Zaikova[2], Kenyon Plummer[2], Thomas Allen[3], James Stasiak[4], Paul Harmon[3], James Hutchison[2], Albrecht Jander[1], Pallavi Dhagat[1]; 1. Oregon State University, Corvallis, OR, USA; 2. University of Oregon, Eugene, OR, USA; 3. Voxtel Inc., Beaverton, OR, USA; 4. HP Labs, Inc., Corvallis, OR, USA

Abstract

The fabrication of composite materials having digitally designed dielectric and magnetic properties varying on a voxel-by-voxel basis offers exciting prospects for additive manufacturing of gradient index lenses for radio frequency (RF) signals. Such lenses will, in the future, be custom printed to form application-specific beam patterns in RF communications systems such as cellular telephone, Wi-Fi, radar, and internet of things (IoT). Here we present materials and methods for the digitally controlled additive manufacturing of magneto-dielectric composites with dielectric permittivity and magnetic permeability programmable on a voxel-by-voxel basis.

Introduction

The future radio wave landscape looks crowded, with personal communications (cell phones, Wi-Fi, Bluetooth), autonomous vehicles (radar, vehicle-to-vehicle and vehicle-to-road communications), and wireless internet-connected devices (the so-called "internet of things") competing for limited radio frequency (RF) spectrum. To conserve the RF spectral resources, as well as the power in mobile devices, each device may require a custom-designed antenna beam pattern. This presents an opportunity for digital manufacturing of application-specific gradient index RF lenses to shape and direct the antenna beam.

In this paper, the materials, processing, and characterization techniques required to produce functional gradient index (GRIN) RF lenses using digital and additive manufacturing methods are discussed. The design of the lenses is based on transformation optics (TO) approaches [1, 2], in which the shape of the input beam and the desired shape of the output beam are used to algorithmically determine the required spatial distribution of refractive index, $n(x,y,z)$, for the gradient index lens [3, 4]. Existing literature considers varying only the dielectric permittivity, ε, of the lens material. However, additionally varying the magnetic permeability, μ, of the lens material would allow independent control of the wave impedance, $Z = \sqrt{\mu/\varepsilon}$, as well as the refractive index $n \sim \sqrt{\mu\varepsilon}$, enabling impedance matching and reduction of unwanted reflections.

An example of a gradient index lens designed by TO methods is shown in Fig. 1. The electromagnetic wave simulation shows the otherwise hemispherical radiation from a patch antenna being collimated into a beam by use of a graded refractive index cylindrical lens. In this design, the relative permittivity and permeability were constrained to a conservative range of 1 to 5 and 1 to 2.5 respectively. In contrast to an equivalent lens with gradients in permittivity only (requiring values up to 7.5) this lens has lower reflection losses at the lens surface. Additive manufacturing of such a lens will require voxel-by-voxel control of the permittivity and permeability of the material being incorporated into the structure.

Ultimately, the focusing ability and size reduction of the lens antenna are limited by the range of refractive index (contrast ratio) that can be achieved in the additive manufacturing process. A larger ratio of maximum to minimum refractive index enables more compact lens designs and higher antenna gain to be achieved. Thus, a key goal of our work is not only to fabricate objects with pre-determined refractive index gradients, but also to maximize the possible contrast ratio.

Additive Manufacturing Methods

To ultimately realize small, high gain lenses, the focus of this project has been to develop materials and additive manufacturing processes to incorporate well-controlled fractions of high-permittivity and high-permeability nanoparticles into 3D printed objects. We develop two unique additive manufacturing methods for variable permeability/permittivity functional materials:

1. **Polymer particle bed infiltration and fusing,** in which solutions carrying functional dielectric or magnetic nanoparticles are infiltrated into a polymer powder bed using inkjet printing. Each layer of powder is fused by heating above the melting temperature of the polymer. The object permeability and permittivity are determined by digitally controlling the amount of solution that is infused in each printed voxel.
2. **Inkjet printing of a polymerizable nanocomposite ink**, in which suspensions of dielectric or magnetic nanoparticles in a

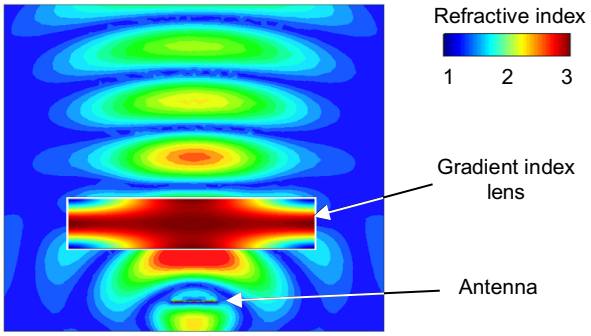

Figure 1. *Electromagnetic wave simulation of a gradient index RF lens designed by transformation optics under the constraint of $\varepsilon < 5\varepsilon_0$ and $\mu < 2.5\mu_0$. The initially radially diverging beam from the antenna (see below the lens), operating at 2.4 GHz, is collimated to a parallel beam by the lens (see above the lens). The lens is 25 cm in diameter and 6.25 cm in thickness.*

UV-polymerizable matrix solution are printed one layer at a time followed by curing with UV light. The object permeability and permittivity are determined by digitally controlling the ratio of three different "colors" of ink that are jetted into each voxel, i.e. inks containing dielectric nanoparticles, magnetic nanoparticles, or polymer matrix only.

Polymer particle bed infiltration and fusing

In this technique digital inkjet printing and powder bed fusion processing are integrated to produce functional polymer nanocomposites with predictable and reproducible dielectric properties. Dielectric polymer nanocomposites are fabricated using commercial grade polyamide 12 (PA12) powder (HP 3D High Reusability PA 12) [5]. An ink containing a stabilized dispersion of barium titanate ($BaTiO_3$) nanoparticles was formulated and dispensed into the PA12 powder using a thermal inkjet materials printer. The nanoparticles were synthesized using the mixed-oxide solid-state reaction method [6]. X-ray diffraction measurements confirmed that the nanoparticles had a composition of $Ba_1Ti_{1.1}O_4$ i.e., near the correct stoichiometry though slightly rich in Ti.

Functionalization of the nanoparticles using ligand-attachment chemistry is used to reduce aggregation of the nanoparticles in the ink solvent [7]. The functionalization process also serves to increase the molecular-scale attachment rates and retention efficiency between the infiltrating nanoparticles and the surfaces of the wetted PA12 particles, resulting in a more homogeneous distribution of nanoparticles within the powder layer [8, 9].

The fabrication system is illustrated in Fig. 2. In this study, the volume fraction of $BaTiO_3$ nanoparticles that infiltrated the PA12 powder was controlled using an automated printing program. Following the inkjet printing step, the powder sample was heated above the PA12 melting temperature (~188.5°C) using radiant heating and then allowed to cool to room temperature. A layer-by-layer approach was used, in which successively a fresh layer of powder (~100 microns thick) was applied, mechanically smoothed, and packed on top of the previously fused layer and then infused with the $BaTiO_3$ ink. This process was repeated until a ~2 mm thick sample was produced. Using multiple passes to fill the interstitial spaces of the loosely packed powder, a volumetric loading of up to 45% $BaTiO_3$ could be achieved. After fusing, 1 cm diameter Au electrodes were deposited onto both sides of each sample to facilitate electrical characterization.

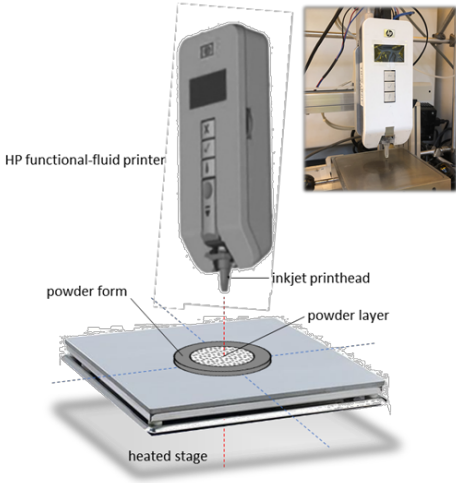

Figure 2. *Schematic illustration of the printing system used to fabricate the dielectric polymer nanocomposite samples. The system includes an experimental printer developed by HP. A photograph of the system is shown in the inset.*

Cross-sections through four polymer nanocomposite samples prepared by the powder bed fusion technique are shown in Fig. 3. Each photograph represents a different volume fraction of $BaTiO_3$ nanoparticles. In the photographs, clusters of ~100 nm aggregates mixed into the polymer are visible. Although the sample cross-sections are still being analyzed, it is likely that clusters are formed by aggregated groups of nanoparticles dispersed into the PA12 polymer host.

Inkjet printing of polymerizable nanocomposite ink

In the second approach, samples were prepared by piezoelectric inkjet printing of dielectric (barium titanate) or magnetic (barium hexaferrite) nanoparticles suspended in a UV-cured diethylene glycol diacrylate (DEGDA) matrix [10]. Commercially available nanoparticles were used in the case of $BaTiO_3$ (99.95% purity, 50 nm and 100 nm diameters, Inframat Advanced Materials). Barium hexaferrite nanoparticles were synthesized following Temuujin et al. [11] with modifications to target the Co_2Z phase ($Ba_3Co_2Fe_{24}O_{41}$), which has the desirable property of high permeability at high frequencies. Briefly, powders of $BaCO_3$ (1 µm powder, Alfa Aesar, Cat # 14341), Co_3O_4 (50 nm–80 nm powder, Alfa Aesar, Cat # 44661), and α-Fe_2O_3 (30 nm–50 nm powder, Alfa Aesar, Cat # 47044) in the molar ratio 3:2/3:12, respectively, were ball milled at 300 rpm for 20 h in ethanol. The resulting powder was annealed for 4 h at 1230 °C in air and subsequently ball milled for 7 h at 500 rpm. The final material is partially Co_2Z phase as confirmed by x-ray diffraction. The data are shown in Fig. 4, in comparison to published results by Tachibana et al. [12].

The inks were prepared by first functionalizing the nanoparticles with acrylic acid. Acrylic acid can effectively integrate the nanoparticles into the matrix material since it can polymerize with the DEGDA and also has a carboxylic acid group

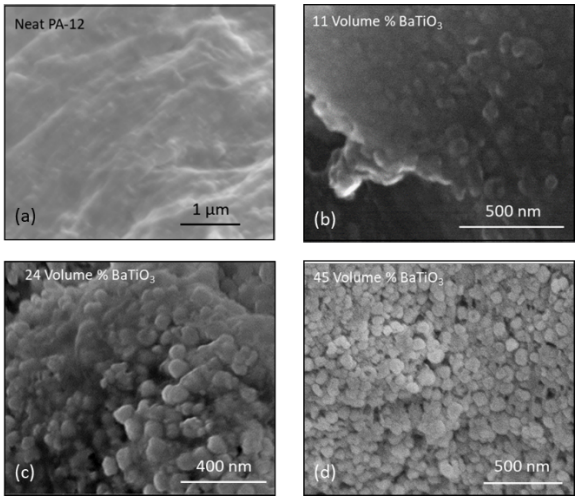

Figure 3. *Micrographs of cross-sections through the dielectric samples at four different $BaTiO_3$ volume fractions in the PA12 matrix. (a) no fillers, (b) 11%, (c) 24% and (d) 45%.*

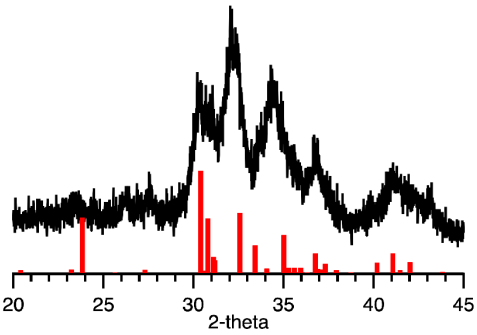

Figure 4. *X-ray diffraction pattern of the synthesized barium hexaferrite nanoparticles (black) with z-phase peak intensities for reference (red).*

capable of binding to the nanoparticle surface. To functionalize, the nanoparticles (1 g) were milled with zirconia balls (~70 g) in a planetary ball-mill (Retsch PM100) for 1 h at 500 rpm with acrylic acid (0.5 mL) and ethanol (15 mL). Thereafter, the mixture was purified by repeated rinsing in ethanol, centrifugation and decanting. Finally, a known volume of ethanol (about 5 mL for every 1 g of nanoparticles) was added to the solid immediately after decanting and sonicated for 1 h. The amount of DEGDA required to achieve the desired nanoparticle concentration was added to the dispersion, and the ethanol was evaporated using a rotary evaporator. The final dispersion of nanoparticles in DEGDA was sonicated daily until casting samples or 3D printing. Immediately prior to use, an initiator (Irgacure 184) was added at 3 wt% (relative to monomer) to the dispersion, which was then sonicated for about 30 minutes.

3D printing was carried out with a Dimatix Materials Printer DMP-2850. Nanoparticle-DEGDA dispersions were loaded into the Dimatix Materials Cartridge consisting of 16 square piezoelectric nozzles spaced 254 µm apart. The nozzles have an effective diameter of 21 µm with drop volumes of about 10 pL. A small spot size UV LED light (365 nm wavelength) attached to the printer head

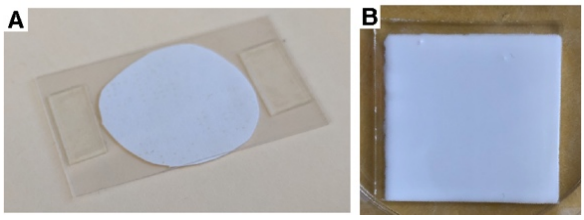

Figure 5. *Example images of cast and printed composite samples. Composite sample is shown in the slide assembly used to cast samples (A). Composite sample is shown on glass substrate after 3D printing (B).*

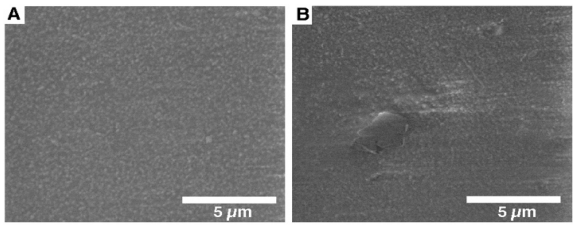

Figure 6. *SEM images of surfaces of 3D printed composites prepared from 50 nm $BaTiO_3$ nanoparticles at weight fractions of 10% (A) and 20 % (B).*

was used for curing by passing over the printed area in a raster pattern. Inks were printed at room temperature in a nitrogen environment onto a piranha-cleaned glass substrate in the pattern of a 3 cm square via a sequence of depositing the ink and curing with UV light. Specifically, two layers of ink were deposited followed by two passes with UV light. This cycle was repeated in order to build up a thicker sample. Each cycle increased the thickness of the sample by approximately 20 µm.

Inks with high concentration of nanoparticles tend to quickly clog the inkjet print head. Therefore, the key to achieving a high volumetric fraction of nanoparticles in the final object, while still allowing inkjet printing, is to dilute the ink with a solvent (dimethylformamide) that evaporates prior to initiating the polymerization of the DEGDA. Using this approach, a volume

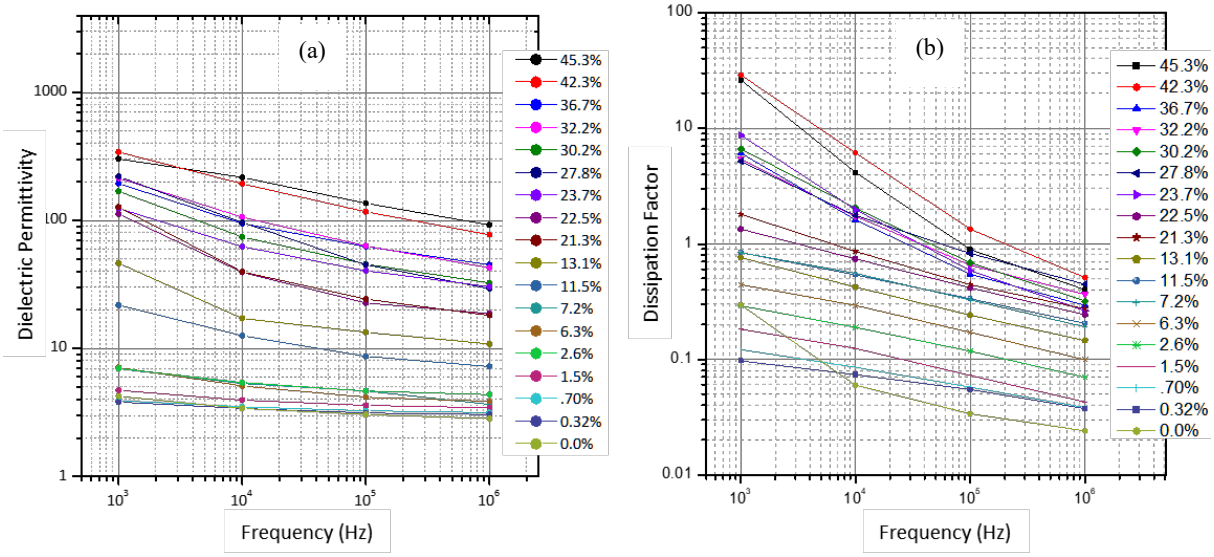

Figure 7. *Frequency dependent dielectric properties of samples manufactured by polymer bed infusion, parametric in the $BaTiO_3$ volume fraction. (a) the dielectric constant ε' and (b) the dissipation factor ε''.*

fraction as high as 50% in the printed and cured samples was achieved.

Since the printing process with the experimental inkjet printer is quite slow, additional samples were prepared by casting. Two glass slide coverslips were separated using small strips of double-sided tape [13]. About 150 µL to 250 µL of nanoparticle-DEGDA dispersion was placed on a coverslip between two narrow strips of double-sided tape and the second slide was placed on top (Fig. 5A). The thickness of the sample could be increased by having multiple layers of tape. This assembly was placed under UV light for about 5 minutes, flipped over, and exposed for another 5 minutes to cure. The cured samples could be removed from the glass slides using a razor blade. Photographs of both cast and printed samples are shown in Fig. 5. SEM images of the surface of inkjet printed samples are shown in Fig. 6.

Results

The polymer nanocomposite samples were characterized using impedance spectroscopy techniques [14] to determine the complex permittivity $\varepsilon = \varepsilon' - i\varepsilon''$ as functions of the $BaTiO_3$ nanoparticle volume fraction. The permittivity is determined from capacitance measurements at frequencies between 100 Hz and 1 GHz. All measurements were made at room temperature.

For the fused powder bed polymer nanocomposites, the dielectric constant ε' and the dissipation factor ε'' as a function of frequency for different volume fraction of $BaTiO_3$ are plotted in Fig. 7. A general feature is the systematic decrease of both the dielectric constants and dissipation factors with increasing frequencies with the slopes becoming steeper with increasing volume fractions. This frequency dependence of both the real ε' and imaginary ε'' relative permittivity is consistent with the predictions of the Maxwell-Wagner-Sillars (MWS) theory [15, 16] describing the dielectric properties of two-phase inhomogeneous media including contributions from the dielectric relaxation of the composite medium, the shapes, sizes, and orientations of the filler particles, and polarization effects at microscopic and macroscopic interfaces.

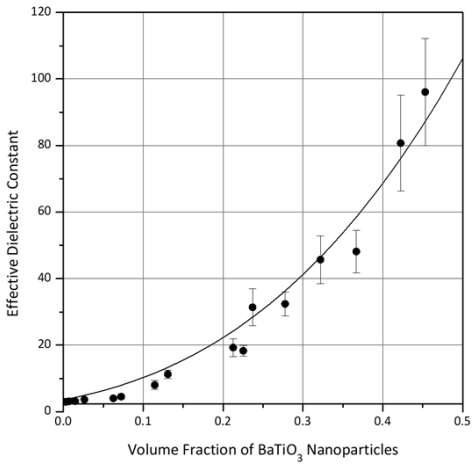

Figure 8. *The effective dielectric constant of a $BaTiO_3$ polymer nanocomposite sample at 1 kHz versus nanoparticle volume fraction. The data points represent the average of at least 5 measurements and the error bars are ± 1σ. The solid line is a curve fit using the Looyenga power-law mixing equation.*

The measured dependence of the dielectric constant on the nanoparticle volume fraction is shown in Fig. 8. The data are fit using a power-law effective medium "mixing equation" that has been used to model the properties of a wide range of nanocomposite materials [17]:

$$\varepsilon_{eff}^{1/\beta} = f\varepsilon_i^{1/\beta} + (1-f)\varepsilon_e^{1/\beta} \quad (1)$$

in which f is the volume fraction, ε_{eff}, ε_i, and ε_e are the effective dielectric constant of the composite, the dielectric constant of the filler, and the dielectric constant medium respectively, and the exponent β can be any integer between 1 and 3. Assuming the dielectric constants for the polymer matrix and the $BaTiO_3$ nanoparticles to be 3.6 and 500 respectively, there is a good fit of the data ($R^2 = 0.98$) when $\beta = 3.02$. With $\beta = 3$, the power-law equation corresponds to the well-known Landau-Lifschitz-Looyenga mixing rule [18].

The goodness of the fit of the data in Fig. 8 with an established mixing equation suggests that the physical picture of a polymer matrix homogeneously filled with nanoparticles is reasonable and

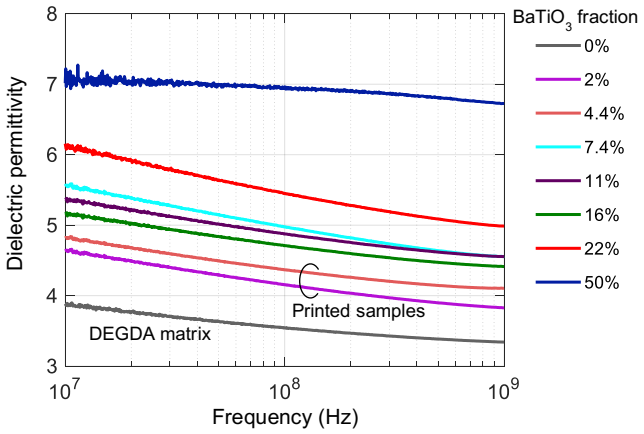

Figure 9. *Dielectric permittivity versus frequency of samples with different $BaTiO_3$ nanoparticle loading (in volume fraction) in DEGDA. The 2% and 4.4% samples were inkjet printed and the remaining prepared by casting.*

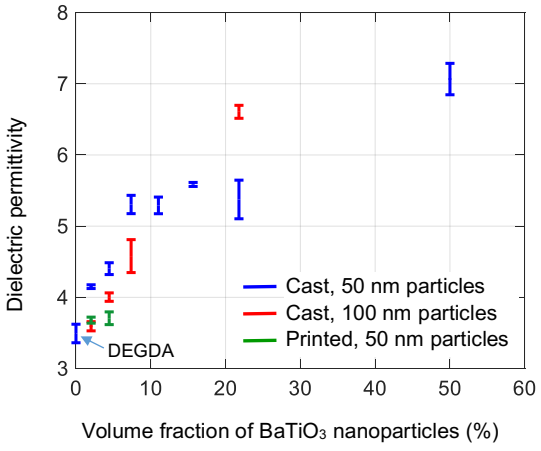

Figure 10. *Dielectric permittivity at 100 MHz versus $BaTiO_3$ nanoparticle loading (in volume fraction) in DEGDA matrix for composite samples prepared by casting and inkjet printing.*

that the procedure used to fabricate polymer nanocomposites with tailored physical properties is promising. Similar mixing rules apply to magnetic composites [19, 20] and consequently, it is assumed that this fabrication process can be used to produce magneto-dielectric materials with digitally-tailored properties.

For the polymer nanocomposite samples prepared by the second technique of printing and UV-curing the ink, representative frequency dependent permittivity is plotted as a function of frequency up to 1 GHz and $BaTiO_3$ fraction in Fig. 9. The permittivity, similar to the observation with powder bed samples, decreases with increasing frequency. The relationship between permittivity at 100 MHz and $BaTiO_3$ fraction for both printed and cast samples is shown in Fig. 10. At this frequency, a contrast ratio of about 2 (7:3.5) is achieved.

The casting method was also used to prepare a sample containing 50% volume fraction of barium hexaferrite nanoparticles in DEGDA. The magnetic permeability of this sample as a function of frequency is shown in Fig. 11. The DEGDA matrix is nonmagnetic (permeability = 1). Thus, the achievable contrast ratio for the magnetic permeability is 1.5 at 100 Hz. This contrast ratio decreases with increasing frequency.

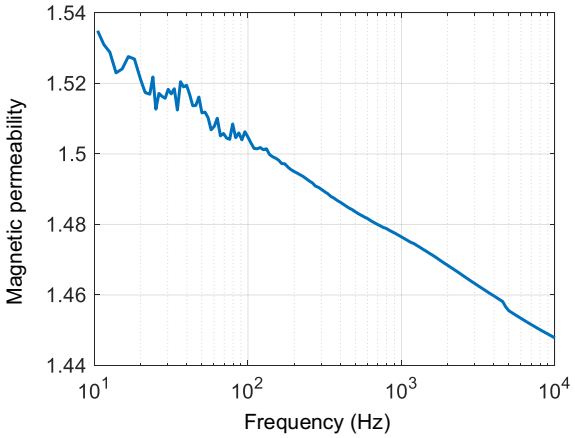

Figure 11. *Magnetic permeability versus frequency for a cast sample containing barium hexaferrite nanoparticles in DEGDA with 50% volume fraction.*

Conclusion

The results from this study demonstrate the possibility of designing and fabricating functional magneto-dielectric composites and 3D devices using digital inkjet printing methods. Two approaches—using particle bed infiltration and fusing, and printing polymerizable nanocomposite inks—were explored. The measured dielectric permittivity of the samples was found to be in qualitative agreement between the two techniques. The permittivity increased with higher nanoparticle volume fraction and decreased with increasing frequency. The good agreement of measured values for the fused samples with the established theory for two-phase composites suggests that it will be feasible to design devices with predetermined electromagnetic properties and hence, performance. Spatial control of permittivity and permeability, enabled by these techniques, will permit TO-designed, application-specific gradient index devices to be rapidly prototyped and fabricated for radar and communication technologies. However, despite the promise, significant challenges must be addressed. In particular, achieving high contrast ratio in permittivity and permeability at radio frequencies will be critical.

Acknowledgement

This work was supported in part by the National Science Foundation (award no. 1611601).

References

[1] J. P. Turpin, A. T. Massoud, Z. H. Jiang, P. L. Werner, and D. H. Werner, "Conformal mappings to achieve simple material parameters for transformation optics devices," *Optics Express*, vol. 18, pp. 244–252, 2010.

[2] N. B. Kundtz, D. R. Smith, and J. B. Pendry, "Electromagnetic design with transformation optics," *Proceedings of the IEEE*, vol. 99, pp. 1622–1633, 2011.

[3] W. Tang, S. Member, C. Argyropoulos, S. Member, and E. Kallos, "Discrete coordinate transformation for designing all-dielectric flat antennas," *IEEE Transactions on Antennas and Propagation*, vol. 58, pp. 3795–3804, 2010.

[4] N. I. Landy, and W. J. Padilla, "Guiding light with conformal transformations," *Optics Express*, vol. 17, pp. 1777–1780, 2009.

[5] H. D. Company, "HP 3D High Reusability PA 12." pp. 1–2, 2017.

[6] M. Kim, S. Schmitt, J. Choi, J. Krutty, and P. Gopalan, "From self-assembled monolayers to coatings: advances in the synthesis and nanobio applications of polymer brushes," *Polymers*, vol. 7, pp. 1346–1378, 2015.

[7] H. Heinz, C. Pramanik, O. Heinz, Y. Ding, R. K. Mishra, D. Marchon, R. J. Flatt, I. Estrela-Lopis, J. Llop, S. Moya, and R. F. Ziolo, "Nanoparticle decoration with surfactants: Molecular interactions, assembly, and applications," *Surface Science Reports*. 2017.

[8] S. Torkzaban, S. A. Bradford, J. Wan, T. Tokunaga, and A. Masoudih, "Release of quantum dot nanoparticles in porous media: Role of cation exchange and aging time," *Environmental Science and Technology*, vol. 47, pp. 11528–11536, 2013.

[9] S. A. Bradford, and S. Torkzaban, "Determining parameters and mechanisms of colloid retention and release in porous media," *Langmuir*, vol. 31, pp. 12096–12105, 2015.

[10] C. Check, R. Chartoff, and S. Chang, "Inkjet printing of 3D nano-composites formed by photopolymerization of an acrylate monomer," *Reactive and Functional Polymers*, vol. 97, pp. 116–122, 2015.

[11] J. Temuujin, M. Aoyama, M. Senna, T. Masuko, C. Ando, and H. Kishi, "Benefits of mild wet milling of the intermediates for the synthesis of phase-pure Z-type hexaferrite," *Journal of Materials Research*, vol. 20, pp. 1939–1942, 2005.

[12] T. Tachibana, T. Nakagawa, Y. Takada, K. Izumi, T. Yamamoto, T. Shimada, and S. Kawano, "X-ray and neutron diffraction studies on iron-substituted Z-type hexagonal barium ferrite: Ba3Co2−xFe24+xO41 (X=0–0.6)," *Journal of Magnetism and Magnetic Materials*, vol. 262, pp. 248–257, 2003.

[13] R. Popielarz, C. K. Chiang, R. Nozaki, and J. Obrzut, “Dielectric properties of polymer/ferroelectric ceramic composites from 100 Hz to 10 GHz,” *Macromolecules*, vol. 34, pp. 5910–5915, 2001.

[14] J. R. Macdonald, and W. B. Johnson, “Fundamentals of impedance spectroscopy,” in *Impedance Spectroscopy: Theory, Experiment, and Applications, Second Edition*, Hoboken, NJ: John Wiley and Sons, Inc., 2005.

[15] L. K. H. Van Beek, “The Maxwell-Wagner-Sillars effect, describing apparent dielectric loss in inhomogeneous media,” *Physica*, vol. 26, pp. 66–86, 1960.

[16] H. Lu, X. Zhang, and H. Zhang, “Influence of the relaxation of Maxwell-Wagner-Sillars polarization and dc conductivity on the dielectric behaviors of nylon 1010,” *Journal of Applied Physics*, vol. 100, 054104, 2006.

[17] A. H. Sihvola, *Electromagnetic mixing formulas and applications*. London: The Institution of Electrical Engineers, 1999.

[18] H. Looyenga, “Dielectric constants of heterogeneous mixtures,” *Physica*, vol. 31, pp. 401–406, 1965.

[19] H. Sharma, S. Jain, P. M. Raj, and K. P. Murali, “Magnetic and dielectric property studies in Fe- and NiFe-based polymer nanocomposites,” *Journal of Electronic Materials*, vol. 44, pp. 3819–3826, 2015.

[20] G. Clay, H. Song, J. Nielsen, J. Stasiak, M. Khavari, A. Jander, and P.Dhagat, “3D printing magnetic material with arbitrary anisotropy,” *NIP31/Digital Fabrication 2015 Conference Proceedings*, no. 1, pp. 307–310 2015.